NeuroImage **14,** 531–545 (2001)
doi:10.1006/nimg.2001.0830, available online at http://www.idealibrary.com on IDEAL®

Statistical Analysis of Hippocampal Asymmetry in Schizophrenia

Lei Wang,*[,1] Sarang C. Joshi,† Michael I. Miller,‡ and John G. Csernansky*[,§]

Received July 26, 2000

*Department of Psychiatry, Washington University School of Medicine, St. Louis, Missouri 63110; †Departments of Radiation Oncology and Biomedical Engineering, University of North Carolina, Chapel Hill, North Carolina; ‡Center for Imaging Science, Whiting School of Engineering, The Johns Hopkins University, Baltimore, Maryland 21218; and §Metropolitan St. Louis Psychiatric Center, St. Louis, Missouri 63130

The asymmetry of brain structures has been studied in schizophrenia to better understand its underlying neurobiology. Brain regions of interest have previously been characterized by volumes, cross-sectional and surface areas, and lengths. Using high-dimensional brain mapping, we have developed a statistical method for analyzing patterns of left–right asymmetry of the human hippocampus taken from high-resolution MR scans. We introduce asymmetry measures that capture differences in the patterns of high-dimensional vector fields between the left and right hippocampus surfaces. In 15 pairs of subjects previously studied (J. G. Csernansky *et al.*, 1998, *Proc. Natl. Acad. Sci. USA* 95, 11406–11411). we define the difference in hippocampal asymmetry patterns between the groups. Volume analysis indicated a large normative asymmetry between left and right hippocampus (R > L), and shape analysis allowed us to visualize the normative asymmetry pattern of the hippocampal surfaces. We observed that the right hippocampus was wider along its lateral side in both schizophrenia and control subjects. Also, while patterns of hippocampal asymmetry were generally similar in the schizophrenia and control groups, a principal component analysis based on left–right asymmetry vector fields detected a statistically significant difference between the two groups, specifically related to the subiculum.

INTRODUCTION

Evidence of structural asymmetry in the human brain has been documented in the literature extensively for the past several decades. In 1968, Geschwind and Levitsky (1968) studied postmortem human brains and observed that the size of the left planum temporale was larger than the right. In 1977, after dissecting and studying over 100 postmortem brains, Kopp and colleagues (1977) concluded that "anatomical asymmetries of the two cerebral hemispheres in man seem to be numerous."

The advent of computerized imaging technology over the past few decades has enabled researchers to identify and measure brain asymmetries *in vivo*, via modalities such as computer-assisted tomography (CT) (LeMay, 1976, 1977; LeMay and Kido, 1978), positron emission tomography (PET) (Luxenberg *et al.*, 1987; Wu *et al.*, 1991; Lotspeich and Ciaranello, 1993), magnetic resonance imaging (MRI) (Kulynych *et al.*, 1993; Peled *et al.*, 1998; Dickey *et al.*, 1999), and functional MRI (Mottaghy *et al.*, 1999). Using these technologies, researchers have been able to observe volumetric asymmetries in the temporal (Jack *et al.*, 1988; Loftus *et al.*, 1993; Lee *et al.*, 1995), frontal, and occipital lobes (Galaburda *et al.*, 1978; Andreasen *et al.*, 1982; Glicksohn and Myslobodsky, 1993), as well as cortical gyri (Wible *et al.*, 1995; Szeszko *et al.*, 1999), thalamus (Eidelberg and Galaburda, 1982), and basal ganglia (Tien *et al.*, 1996). For example, the right frontal lobe is often larger than the left, while the right occipital lobe is smaller than the left (Weinberger *et al.*, 1982). Comparisons of normal versus abnormal asymmetries may give us insights into the neurobiology of schizophrenia (Bullmore *et al.*, 1995; James *et al.*, 1999), degenerative dementia (e.g., Alzheimer's disease (Luxenberg *et al.*, 1987; Thompson *et al.*, 1998)), and other neuropsychiatric illnesses such as autism (Lotspeich and Ciaranello, 1993) and personality disorder (Dickey *et al.*, 1999).

With regard to the hippocampal volumes, Pruessner *et al.* (2000) pointed out that results were "inconsistent with regard to interhemisphereic differences," but that the vast majority of the studies suggested either normative R > L asymmetry or no left–right differences. Moreover, research on hippocampal asymmetry in the context of neuropsychiatric illnesses such as schizophrenia, Alzheimer's disease (AD), and epilepsy (Hirayasu *et al.*, 1998; Galderisi *et al.*, 1999; Moossy *et al.*,

[1] To whom correspondence should be addressed at Department of Psychiatry, Washington University School of Medicine, Campus Box 8134, 660 S. Euclid Avenue St. Louis, MO 63110. Fax: (314) 747-6267. E-mail: lei@klebit.wustl.edu.

1053-8119/01 $35.00

1988; Cook *et al.*, 1992; Lawson *et al.*, 1998; Hogan *et al.*, 1999) may be even less adequate. In schizophrenia, the majority of the MRI literature suggests that the R > L asymmetry present in normal individuals is exaggerated among schizophrenia subjects (Hirayasu *et al.*, 1998; Galderisi *et al.*, 1999). However, some older CT studies suggested a "reversal of asymmetry" (Luchins *et al.*, 1979; Andreasen *et al.*, 1982), while others observed the same level of asymmetry as controls (Kulynych *et al.*, 1995).

Historically, patterns of brain asymmetry has been measured using a "left–right asymmetry index": $1 (l - r) / 2 (l + r)$ (Eidelberg and Galaburda, 1982; Pieniadz and Naeser, 1984). This formula has been applied to volume, length, and cross-sectional and surface area calculations. However, such calculations make a summary comparison between the left and right brain structures of interest and ignore the possibility of subregional differences. While a change in the pattern of asymmetry may not be detectable for the whole structure, *significant* regional asymmetries may remain undiscovered. Structural changes in schizophrenia when compared with control subjects are subtle yet significant (Csernansky *et al.*, 1998), and the differences in asymmetry patterns may be even more subtle. Furthermore, the development of brain atlases (Collins *et al.*, 1994), high-dimensional brain mapping (HDBM) (Miller *et al.*, 1993; Christensen *et al.*, 1994, 1996, 1997; Grenander and Miller, 1994; Miller *et al.*, 1997; Joshi *et al.*, 1995), and probabilistic models of brain anatomies as connected surface meshes (Thompson *et al.*, 1996) make it possible to quantify the variability of cortical and subcortical brain structures and to compare subtleties in brain anatomies. Joshi and colleagues (Joshi *et al.*, 1997) modeled populations of hippocampi as surfaces derived from a common template via HDBM. They pioneered the methods of assessing the "shape" of the hippocampal surface by computing statistics associated with three-dimensional vector transformation fields across the entire hippocampal surface. These technological advances now make it possible to compare subtleties between population groups via "shape" rather than overall volume.

We now apply the analysis of shape to the problem of quantifying hippocampal asymmetry in a controlled study of schizophrenia, in which left and right hippocampi of each subject were mapped from a common template. Using hippocampal volume, a strong hemispheric asymmetry was previously found for all subjects combined (Csernansky *et al.*, 1998). However, there was no significant group×hemisphere interaction; i.e., the difference in hippocampal volume asymmetry was not large enough to set the two groups apart.

In this study, we first precisely define hippocampal asymmetry as a vector field resulting from a flipping group action and introduce techniques for the visualization of asymmetry patterns along the hippocampal surfaces. We then put forth a statistical measure of individual and group asymmetry. Finally, we compare the asymmetry patterns to statistically discriminate the two groups of subjects.

SUBJECTS AND METHODS

The subject and template scans used in this work came from our previously published study of hippocampal morphometry in schizophrenia (Csernansky *et al.*, 1998). In that study, 15 subjects with schizophrenia and 15 healthy controls gave informed consent to MR scanning after the risks and benefits were explained. MR scans were obtained by using a Siemens Magnetom SP-4000 1.5-T imaging system, a standard head coil, and a magnetization prepared rapid gradient echo (MP_RAGE) sequence (TR/TE, 10/4; ACQ, 1; matrix, 256×256; scanning time, 11.0 min). The sequence produced three-dimensional data sets with 1 × 1-mm in-plane resolution and 1.25-mm slice thickness across the entire cranium. The template hippocampus was developed in previous work (Haller *et al.*, 1997) and was mapped onto the left and right sides of each subject via HDBM. Refer to Csernansky *et al.* (1998) for further details of subject recruitment, MR acquisition, and the mapping of the hippocampus. The definition of the template hippocampus including the subiculum is detailed in Appendix A.

The mathematical methods of HDBM for studying brain variabilities were introduced by Grenander and Miller (1998) in the new emerging discipline of *computational anatomy*. Governed by Grenander's pattern-theoretic principles (Grenander, 1970, 1994), neuroanatomies are represented as deformable templates—collections of 0,1,2,3-dimensional manifolds. Anatomic variabilities are then modeled as random (e.g., Gaussian) transformations applied to the template manifold. The anatomic model used herein is a quadruple $(\Omega, \mathcal{H}, \mathcal{I}, \mathcal{P})$, with the template brain coordinate space $\Omega \subset \mathbb{R}^3 = \cup_\alpha M_\alpha$ of 0,1,2,3-dimensional manifolds, the set of diffeomorphic transformations on the space $\mathcal{H} : \Omega \leftrightarrow \Omega$, the space of idealized medical imagery $\mathcal{I}$, and $\mathcal{P}$ the family of probability measures on $\mathcal{H}$. The group of diffeomorphic transformations $\mathcal{H}$ is assumed to be rich enough to represent a large family of anatomies while maintaining the topologies of the template manifold.

Variability across individuals is studied through the set of diffeomorphic transformations $h : \Omega \subset \mathbb{R}^3 \leftrightarrow \Omega$:

$$\begin{aligned} h : x = (x_1, x_2, x_3) \in \Omega &\mapsto h(x) \\ &= (h^1(x), h^2(x), h^3(x)) \in \Omega \doteq x - u(x) \\ &= x - (u^1(x), u^2(x), u^3(x)). \end{aligned} \quad (1)$$

It is sometimes convenient to study the transformations in terms of the $u(\cdot)$ fields (i.e., $h(\cdot)$ modulo the

identity map). For a brief description of HDBM procedures see Appendix B.

For bilateral symmetry of brain structures, consider standard mathematical representations known as symmetry groups. Most straightforwardly, let us examine the reflection group $\mathcal{D}$, which expresses axis-flipping symmetry across the sagittal plane. This makes quantitatively precise the notion of left- and right-sided brain symmetry, as well as variation away from left- and right-side symmetry (i.e., asymmetry) (Grenander and Miller, 1998).

Begin by embedding the human brain in Ω, the unit cube with coordinates

$$x = (x_1, x_2, x_3);\ -\frac{1}{2} \le x_1 \le \frac{1}{2};\quad -\frac{1}{2} \le x_2 \le \frac{1}{2};\ -\frac{1}{2} \le x_3 \le \frac{1}{2}. \tag{2}$$

For simple symmetry across the midsagittal plane, we choose the convention that the midsagittal plane P_{sag} through the center of the longitudinal fissure is the set of all points

$$P_{sag} = \{x = (x_1, x_2, x_3) \in \Omega \mid x_1 = 0\}. \tag{3}$$

The reflection group, $\mathcal{D} = \{I, R\}$, consists of the identity transformation I, the 3×3 identity matrix, and the reflection matrix R across the sagittal plane:

$$D = \left\{ I = \begin{bmatrix} 1 & 0 & 0 \\ 0 & 1 & 0 \\ 0 & 0 & 1 \end{bmatrix}, R = \begin{bmatrix} -1 & 0 & 0 \\ 0 & 1 & 0 \\ 0 & 0 & 1 \end{bmatrix} \right\}.$$

The reflection R generates the following global map across the sagittal plane:

$$R : (x_1, x_2, x_3) \mapsto (-x_1, x_2, x_3). \tag{4}$$

We then redefine the reflection plane across which the symmetry of bilateral brain structures is studied as follows. We use the rigid motions (rotation and translation) to characterize lines and planes of symmetry and define the rigid flip transformation $\{O, R, \mathbf{t} : x \mapsto y = ORx + \mathbf{t}\}$, where O is an orthonormal rotation matrix, R, a reflection matrix with respect to the x axis (the dihedral group), and $\mathbf{t}$ is a translation vector. Then the *plane of symmetry* is the set of points which is invariant to the above transformation; i.e., it is the plane defined by the points which satisfy the equation

$$x = ORx + \mathbf{t}. \tag{5}$$

Once the reflection plane of symmetry has been defined, the notion of left- and right-sidedness, and its quantitative representation becomes straightforward. Examine the transformation from one side to the other side of the brain (i.e., LHS vs RHS),

$$h : x \mapsto h(x) = ORx + \mathbf{t} - u(ORx + \mathbf{t}), \tag{6}$$

with R as the reflection group. If the brain were perfectly symmetric, $u(52)$ would be identically zero. The variation of $u(52)$ away from zero is thus a measure of asymmetry. One should note that while perfect symmetry is defined mathematically to be $u(52) = 0$, we should not expect "normal" asymmetry to be zero. Thus it is the purpose of this study to define normative patterns of asymmetry, as well as the degree to which this normative pattern of asymmetry is distorted in schizophrenia.

Our procedures are as follows:

1. A template of the hippocampus is manually delineated using previously established criteria.
2. The template is aligned with each and every target via landmark-based low-dimensional transformation and then precisely mapped on to the target via intensity-based high-dimensional transformation.
3. Transformation fields are retained for shape analyses across the entire hippocampus surface.
4. Asymmetry maps are obtained by flipping hippocampal surface across a mathematically defined reflection plane in each subject.
5. The measure of asymmetry in the hippocampus is quantified using principal component analysis (PCA).
6. The correspondence between PCA and representative asymmetry patterns are assessed and visualized.
7. The difference in asymmetry patterns between groups is compared.

HIPPOCAMPAL ASYMMETRY

Starting with a template anatomy, the family of M mappings from the template to both sides (to M subjects) is given by

$$\begin{matrix} h_i^l : x \in \Omega \mapsto h_i^l(x) \in \Omega \\ h_i^r : x \in \Omega \mapsto h_i^r(x) \in \Omega \end{matrix}, \quad i = 1, \ldots, M. \tag{7}$$

By supposing that we are flipping from the right to left side (left to right is just the mathematical inverse), each flipping is then defined by (see Eqs.(5) and (6))

$$f_i : x \mapsto OR(h_i^r(x)) + \mathbf{t}, \quad i = 1, \ldots, M. \tag{8}$$

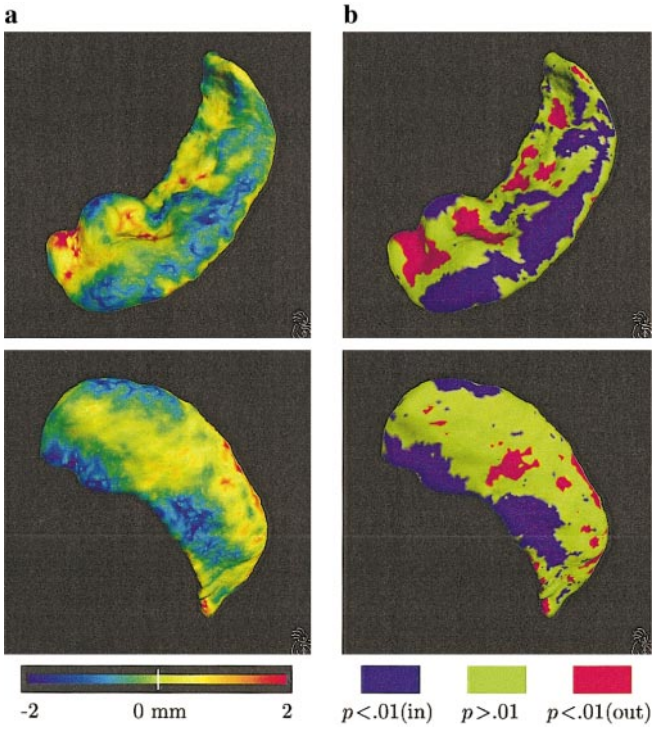

FIG. 1. Normative asymmetry measures of the hippocampal surface visualized on the mean flipped right-side surface. (Top row) Top view of (a) normal component map and (b) Wilcoxon's signed rank test map. (Middle row) Bottom view of the maps. (Bottom row) Color scales: (a) deformation (mm), inward in colder colors, outward in warmer colors; (b) significance (Wilcoxon signed rank sum test, $P < 0.01$), inward in purple, outward in red, and nonsignificant deformation ($P > 0.01$) is shown in green.

We define the *asymmetry vector field* for the matched left–right pair of the ith subject as

$$u_i \doteq f_i - h_i^l : x \mapsto OR(h_i^r(x)) + \mathbf{t} - h_i^l, \quad i = 1, \ldots, M. \tag{9}$$

We represent the template hippocampus surface as a two-dimensional surface (Joshi *et al.*, 1997; Joshi, 1997), constructed from a triangulated graph at the external boundary of the hippocampus. The triangulation is obtained using the marching cubes algorithm (Claudio and Roberto, 1994). The surface points are then the vertices of the triangulated graph. To proceed, let $\mathcal{M}_0$ be the template hippocampus surface. Then the mappings of $\mathcal{M}_0$ to the left and right side of each subject i are

$$h_i^l \circ \mathcal{M}_0 \quad \text{and} \quad h_i^r \circ \mathcal{M}_0, \tag{10}$$

and the asymmetry map of the template surface to each subject is given by

$$u_i \circ \mathcal{M}_0 = (f_i - h_i^l) \circ \mathcal{M}_0, \quad i = 1, \ldots, M. \tag{11}$$

Since both the left and the right sides of each subject are mapped from the same template hippocampus surface, we have the 1-to-1 corresponding surface points on both sides for each subject that are necessary for computing u_i, which are the 3D displacement vectors of all the vertices between the left and right (flipped to the left) hippocampal surfaces.

VISUALIZING ASYMMETRY IN NORMALS AND SCHIZOPHRENIA

We examine patterns of asymmetry on a point-by-point basis across the hippocampus surface. Suppose that the entire population under consideration consists of G groups, each having N_g subjects, $g = 1, \ldots, G$. For each group of asymmetry vector fields $u_i(\cdot)$, $i = 1, \ldots, N_g$, we can then examine the vector components which are normal to the surface:

$$u_i^{\perp}(x) \doteq u_i(x) \cdot \hat{n}_i(x)\, d\nu(x), \tag{12}$$

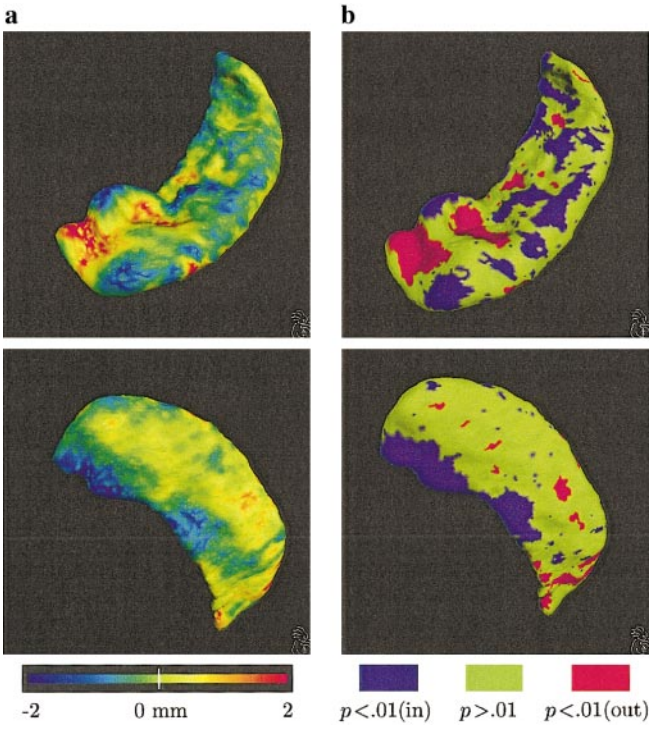

FIG. 2. Asymmetry measures of the hippocampal surface in schizophrenia visualized on the mean flipped right-side surface. (Top row) Top view of (a) normal component map and (b) Wilcoxon's signed rank test map. (Middle row) Bottom view of the maps. (Bottom row) Color scales: (a) deformation (mm), inward in colder colors, outward in warmer colors; (b) significance (Wilcoxon signed rank sum test, $P < 0.01$), inward in purple, outward in red, and nonsignificant deformation ($P > 0.01$) is shown in green.

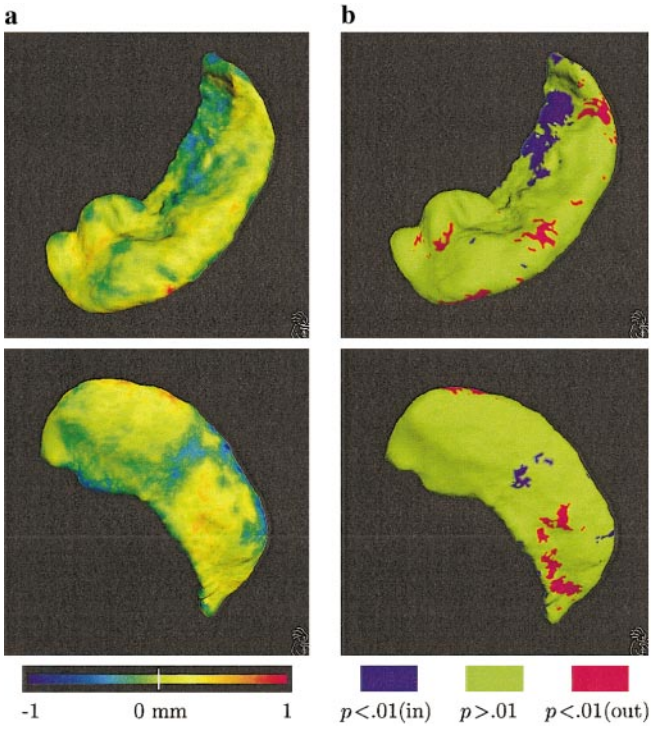

FIG. 3. Difference of hippocampal surface asymmetry patterns between the control and schizophrenia groups visualized on the mean flipped right-side surface of the control group. (Top row) Top view of (a) normal component map and (b) Wilcoxon's signed rank test map. (Middle row) Bottom view of the maps. (Bottom row) Color scales: (a) deformation (mm), inward in colder colors, outward in warmer colors; (b) significance (Wilcoxon signed rank sum test, $P < 0.01$), inward in purple, outward in red, and nonsignificant deformation ($P > 0.01$) is shown in green.

at each surface vertex x across all subjects within the group. Note that $\hat{n}_i(x)$ is the surface normal vector at x and $d\nu(x)$ is the surface measure for M_0 at x. The sample mean then becomes

$$\bar{u}^{\perp}(x) = \frac{1}{N_g} \sum_{i=1}^{N_g} u_i^{\perp}(x). \tag{13}$$

In Fig. 1a, we depict the map of $\bar{u}^{\perp}(\cdot)$ on the mean right hippocampus surface of the control population as the right-side surfaces are flipped to the left side. The top row shows the top view of the map and the middle row shows the view from below. The corresponding color scale (bottom row of Fig. 1a) shows the amount of average asymmetry. Visualizing the actions of asymmetry vector field in this manner allows us to see, on average, where the surfaces are deformed inward due to asymmetry (shown in colder colors) and outward (in warmer colors), as well as areas which are little deformed (in neutral yellow to green colors).

We then examine the significance of these per-point differences without assuming *a priori* knowledge of the distribution of $u_i^{\perp}$, $i = 1, \ldots, N_g$. The significance levels (P values) are computed using the Wilcoxon signed rank sum test (Wilcoxon, 1945) as follows: At each surface vertex x, we compute the signed rank order $u_i^{\perp}(x)$ over all N_g matched left–right pairs after taking out possible $u_i^{\perp} = 0$. The positive and negative ranks are then summed separately. The sum smaller in magnitude (with its sign) is used to look up in the Wilcoxon signed rank exact distribution[2] with one-tailed statistics.[3] The resulting significance is the P value to reject the null hypothesis that the group of asymmetry components is of zero mean, and upon rejection, the one-

[2] We compute the exact distribution into an offline look-up table instead of approximating for large N. The computation procedure is described in http://www.psych.cornell.edu/Darlington/wilcoxon/wilcox0.htm.

[3] One-tailed statistics is used here since it gives a signed significance: negative quantities indicate significant inward deformation and positive quantities indicate significant outward deformation.

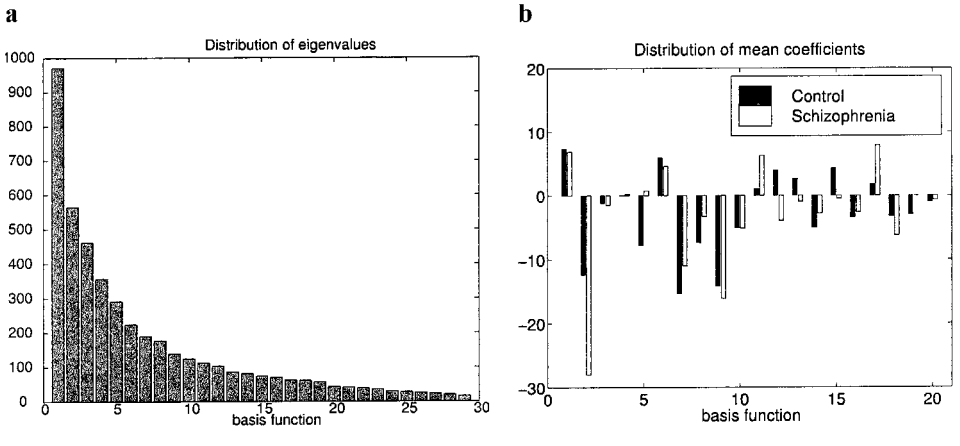

FIG. 4. Principal component analysis of asymmetry vector fields. (a) The distribution of eigenvalues for all basis functions. (b) The distribution of mean coefficients (control and schizophrenia groups) associated with the first 20 basis functions.

TABLE 1

Asymmetry Measures for the Control Group and the Group of Schizophrenia Associated with One Basis Function

	Control		Schizophrenia	
Basis function	Asymmetry measure	Significance of asymmetry (df = 1,14)	Asymmetry measure	Significance of asymmetry (df = 1,14)
1	0.22	P = 0.39 (F = 0.78)	0.21	P = 0.42 (F = 0.68)
2	0.53	P = 0.058 (F = 4.25)	**1.20**	P = **0.0004** (F = 21.83)
3	0.05	P = 0.84 (F = 0.04)	0.06	P = 0.80 (F = 0.06)
4	0.00	P = 0.99 (F = 0.00)	0.01	P = 0.96 (F = 0.00)
5	0.45	P = 0.10 (F = 3.10)	0.04	P = 0.86 (F = 0.03)
6	0.38	P = 0.16 (F = 2.20)	0.29	P = 0.26 (F = 1.32)
7	**1.08**	P = **0.0009** (F = 17.66)	**0.77**	P = **0.0092** (F = 9.11)
8	0.54	P = 0.05 (F = 4.39)	0.24	P = 0.36 (F = 0.88)
9	**1.16**	P = **0.0005** (F = 20.35)	**1.32**	P = **0.0002** (F = 26.27)
10	0.43	P = 0.11 (F = 2.89)	0.44	P = 0.10 (F = 2.95)
11	0.09	P = 0.70 (F = 0.15)	0.59	P = 0.036 (F = 5.32)
12	0.41	P = 0.13 (F = 2.59)	0.40	P = 0.13 (F = 2.48)
13	0.27	P = 0.29 (F = 1.17)	0.09	P = 0.70 (F = 0.15)
14	0.53	P = 0.05 (F = 4.37)	0.29	P = 0.26 (F = 1.34)
15	0.50	P = 0.07 (F = 3.80)	0.05	P = 0.83 (F = 0.05)
16	0.39	P = 0.14 (F = 2.38)	0.30	P = 0.25 (F = 1.40)
17	0.24	P = 0.36 (F = 0.88)	**1.04**	P = **0.0012** (F = 16.52)
18	0.40	P = 0.13 (F = 2.52)	**0.78**	P = **0.0088** (F = 9.26)
19	0.39	P = 0.14 (F = 2.32)	0.00	P = 0.99 (F = 0.00)
20	0.14	P = 0.57 (F = 0.32)	0.09	P = 0.71 (F = 0.14)

Note. The first 20 basis functions are tabulated. Components with high degrees of statistical significance are in boldface.

tailed statistic shows whether the group of asymmetry components is less or greater than zero. We repeat this procedure for each and every surface vertex. In Fig. 1b we show the Wilcoxon signed rank sum test map for the control group. Areas of statistically significant surface inward or outward deformation ($P < 0.01$) are shown. We note that these inward and outward areas correspond to the cooler- and warmer-colored areas in Fig. 1a, respectively.

The visualization techniques suggest that the normative left–right asymmetry pattern of the hippocampus is such that the lateral side of the hippocampal body and head is smaller on the left side, while certain degrees of "bending" occur at the hippocampal head and the subiculum.

In Fig. 2, we show the asymmetry pattern of the schizophrenia group, which has a visual similarity to that observed the control group. However, to directly

TABLE 2

Asymmetry Measures for the Control Group and the Group of Schizophrenia Associated with Two Basis Functions

Control			Schizophrenia		
Asymmetry measure	Significance of asymmetry (df = 2,13)	Basis functions	Asymmetry measure	Significance of asymmetry (df = 2,13)	Basis functions
1.58	P = 0.0002 (F = 17.42)	7, 9	1.81	P = 0.0001 (F = 22.99)	2, 9
1.29	P = 0.0013 (F = 11.68)	2, 9	1.72	P = 0.0001 (F = 20.82)	2, 17
1.27	P = 0.0014 (F = 11.39)	9, 14	1.71	P = 0.0001 (F = 20.55)	9, 17
1.27	P = 0.0014 (F = 11.38)	8, 9	1.55	P = 0.0003 (F = 16.73)	9, 18
1.25	P = 0.0016 (F = 11.02)	9, 15	1.52	P = 0.0003 (F = 16.24)	7, 9
1.24	P = 0.0017 (F = 10.79)	9, 10	1.48	P = 0.0004 (F = 15.40)	2, 18
1.24	P = 0.0018 (F = 10.73)	5, 9	1.46	P = 0.0004 (F = 14.91)	9, 11
1.24	P = 0.0018 (F = 10.73)	9, 18	1.40	P = 0.0006 (F = 13.68)	2, 7
1.22	P = 0.0019 (F = 10.53)	9, 16	1.39	P = 0.0006 (F = 13.63)	9, 12
1.22	P = 0.0020 (F = 10.45)	7, 8	1.39	P = 0.0006 (F = 13.62)	2, 11

Note. For each group, from all possible combinations of two basis functions, the top 10 asymmetry measures are tabulated here in descending order.

TABLE 3

Mean Asymmetry Measures for the Control Group and the Group of Schizophrenia

Group	Selected basis functions	Asymmetry measure	Significance of asymmetry
Control	7, 9	1.58	$P = 0.0002$ ($F = 17.42$, $df = 2,13$)
Schizophrenia	2, 9	1.81	$P = 0.0001$ ($F = 22.99$, $df = 2,13$)

compare the asymmetry patterns between the control (g=1) and the schizophrenia (g = 2) groups, difference maps (normal component and signed rank test) between the group means are needed:

$$\bar{u}^{1,\perp} - \bar{u}^{2,\perp}. \tag{14}$$

The difference in the asymmetry patterns of the control and schizophrenia groups is shown in Fig. 3 using the same method of visualization.

Using surface point-by-point shape analysis, we observe that the right hippocampus is wider along its lateral side in both control and schizophrenia groups of subjects. However, while patterns of hippocampal asymmetry are generally similar in both groups, the visualization techniques indicates significant difference between the groups within the subiculum. Schizophrenia subjects appear to show an exaggerated asymmetry pattern in the subiculum compared to controls.

ASYMMETRY MEASURES VIA PRINCIPAL COMPONENT ANALYSIS

To quantify the asymmetries of the hippocampus described by the vector fields u_i for all subjects, we employ PCA on the hippocampal surface, to reduce the dimensionality of the parameter space from the number of surface vertices (6611) to the number of subjects (30 in this study).

TABLE 4

Asymmetry Measures for Each Subject

Control (basis functions: 7, 9)	Schizophrenia (Basis functions: 2, 9)
1.8735	1.9666
2.6935	2.0010
3.1899	4.8043
0.5571	0.9397
0.3323	3.1047
2.5566	3.3013
1.7805	2.7596
1.7112	2.4267
2.1292	1.0294
1.3409	1.4692
1.3472	1.3712
1.9356	4.1831
1.6538	4.0531
2.8727	1.2994
1.8636	6.9622

Again, the population under consideration consists of G groups, each having N_g subjects, $g = 1, \ldots, G$. Joshi *et al.* (1997), Theorem 3, established the PCA on square integrable vector fields on surface manifolds, for zero-mean Gaussian random vector fields. We extend the theorem to the family of asymmetry vector fields $U = \{u_i\}_{i=1}^N$ *on the* C^2 manifold $\mathcal{M}_0$ which have a nonzero mean $\bar{u}^*$. The covariance can be empirically estimated as $\sum_{i=1}^N (u_i(x) - \hat{\bar{u}}^*(x))(u_i(y) - \hat{\bar{u}}^*(y))^T/(N-1)$, $x, y \in \mathcal{M}_0$, where $\hat{\bar{u}}^*$ is the sample mean of the population vector fields.

The random vector field u_i can then be expanded in terms of the set of complete orthonormal basis functions $\{\phi_k(x) : x \in \mathcal{M}_0, k = 1, \ldots, N\}$:

$$u_i(x) = \sum_{k=1}^{N} \alpha_{ik}\phi_k(x), \tag{15}$$

where $\alpha_{ik} = < u_i, \phi_k > = \int_{\mathcal{M}_0} u_i^T(x)\phi_k(x)\, d\nu(x)$ are the coefficients for the ith subject associated with the kth basis function. The basis functions ϕ_k, $k = 1, \ldots, N$ can be computed numerically via the singular value decomposition of the empirically estimated covariance (see Joshi *et al.*, 1997). They completely characterize the asymmetry between left and right hippocampal surfaces.

For each group g, and for all its subjects $i = 1, \ldots, N_g$, let

$$Z_i^g = [\alpha_i^g, \ldots, \alpha_{iN}^g] = [\langle u_i^g, \phi_1\rangle, \ldots, \langle u_i^g, \phi_N\rangle] \tag{16}$$

be the vector coefficients associated with basis functions $\{\phi_1, \ldots, \phi_N\}$. Then we can regard the coefficient fields $\{Z_1^g, \ldots, Z_{N_g}^g\}$ as samples of a random field whose mean is Z^g. All groups are assumed to have common but unknown covariance Σ. The group sample means and pooled sample covariance are then given by

$$\begin{aligned} \hat{\bar{Z}}^g &= \frac{1}{N_g}\sum_{i=1}^{N_g} Z_i^g, \quad g = 1, \ldots, G \\ \hat{\Sigma} &= \frac{1}{\sum_g N_g - G}\sum_g \sum_{i=1}^{N_g} (Z_i^g - \hat{\bar{Z}}^g)(Z_i^g - \hat{\bar{Z}}^g)^T. \end{aligned} \tag{17}$$

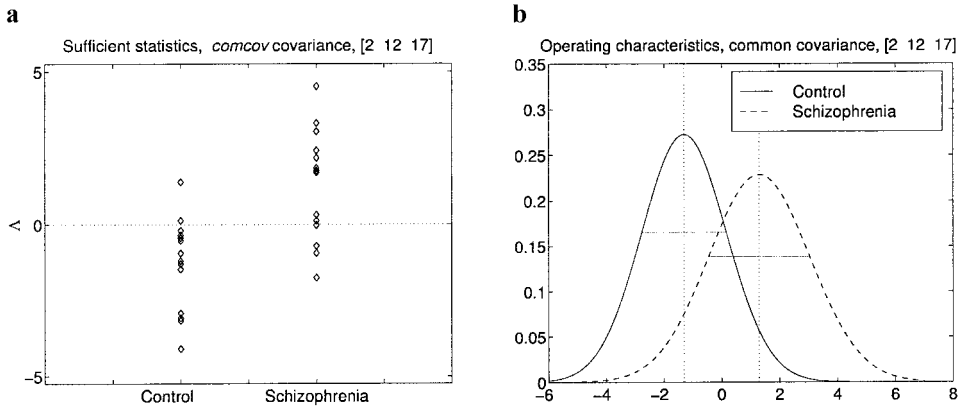

FIG. 5. Principal component analysis of asymmetry pattern differences. (a) Sufficient statistics for a linear combination of basis functions 7, 12, 17. (b) Operating characteristics for the sufficient statistics, with mean and standard deviation for each distribution drawn under the curves.

Asymmetry Measures

For individual group of subjects, the question of whether asymmetry exists (i.e., whether $E(u^g) = 0$) lends itself to a hypothesis test that the vector coefficients for that group have a zero mean (i.e., $E\{Z_1^g, \ldots, Z_{N_g}^g\} = 0$,), assuming an unknown but common covariance. The null hypothesis is therefore

$$H_0 : \bar{Z}^g = 0. \tag{18}$$

Following Theorem 5.2.1 on p. 103 of Anderson (1958), we define the T^2 statistic

$$T^2 \doteq N_g \hat{\bar{Z}}^T \hat{\Sigma}^{-1} \hat{\bar{Z}}^g. \tag{19}$$

If we assume, for group g, that the asymmetry vector field u^g is a random sample from a Gaussian random field, distributed according to $N(\bar{u}^g, K_U)$, then the coefficient field Z^g is also Gaussian, distributed according to $N(\bar{Z}^g, \Sigma)$. From Anderson (1958), T^2 has an F distribution, and the null hypothesis H_0 is rejected with a significance level α if

$$T^2 \geq \frac{(N_g - 1)K}{N_g - K} F^*_{K, N_g - K}(\alpha), \tag{20}$$

where $F^*_{K,N_g-K}(\alpha)$ denotes the upper $100\alpha\%$ point of the F_{K,N_g-K} distribution, and K is the total number of basis functions used in calculating the T^2 statistics.

To quantify the amount of asymmetry for each subject, we define the *asymmetry measure* to be

$$\alpha_i \doteq \sqrt{Z_i^T \hat{\Sigma}^{-1} Z_i}. \tag{21}$$

The mean asymmetry measure for group g is defined to be

$$\bar{a}^g \doteq \sqrt{\hat{\bar{Z}}^{g\,T} \hat{\Sigma}^{-1} \hat{\bar{Z}}_i^g}. \tag{22}$$

Clearly, when $\bar{a}^g = 0$ the group is perfectly symmetric. The larger the value a, the more asymmetry is indicated for the subject or the group. We can interpret this quantity as the distance from zero (which is perfect symmetry) normalized by the covariance.

An Optimal Subset of Basis Functions for Group Asymmetry

The distribution of characteristic values as well as the distribution of mean basis vector coefficients associated with each basis function are shown in Fig. 4. The mean basis vector coefficient for each group is computed according to Eqs. (16) and (17). Its distribution pattern (see Fig. 4b) gives rise to the hypothesis that certain subsets of the basis functions will characterize the asymmetry pattern.

We begin by examining the mean asymmetry measures associated with each basis function. Each of the first 20 basis functions for both groups is shown in Table 1, where the components associated with a highly significant statistical difference from the null hypothesis (i.e., zero asymmetry) are shown in boldface. Notice the correspondence between the selection of these components and the distribution patterns shown in Fig. 4b. After examining all possible combinations of two basis functions, combinations yielding the strongest rejection of the null hypothesis in each group are shown in Table 2, in descending order. Additional basis vectors did not improve the significance of null hypothesis rejection. Using the two-vector combinations (i.e., {7,9} for the control group and {2,9} for the schizophrenia group) that produced the highest level significance asymmetry, we summarize in Table 3 the mean asymmetry measures and the significance levels of asymmetry. We conclude that as a group,

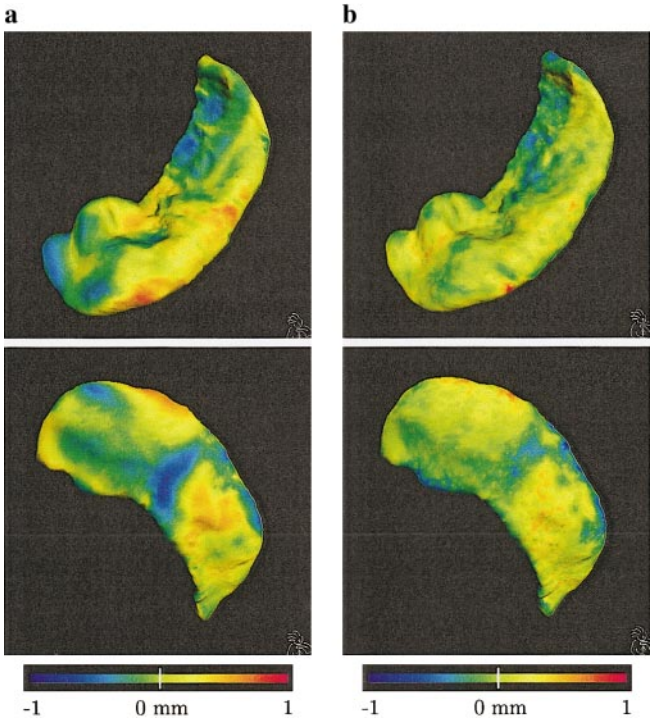

FIG. 6. Difference of hippocampal surface asymmetry patterns between the control and schizophrenia groups expressed in the subset basis functions 2, 12, 17, visualized on the mean of the flipped right-side surface of the control group. (Top row) Top view of normal component maps of (a) asymmetry vector field synthesis and (b) mean group difference, reproduced from Fig. 3a as a visual reference. (Middle row) Bottom view of the maps. (Bottom row) Color scales: (a,b) Deformation (mm), inward in colder colors, outward in warmer colors.

schizophrenia subjects have exaggerated asymmetries compared to the control subjects. The locations of asymmetry in each of these two groups as well as the difference in asymmetry patterns are visualized in Figs. 1–3. Finally, in Table 4 we tabulate asymmetry measures for each subject.

Comparing Asymmetry Patterns between Two Groups

Again, the population under study can be grouped into N_1 number of controls and N_2 number of patients. The group asymmetry is then quantified as in Section 5, and we can now express the difference in the asymmetry patterns between these two groups.

From Section 5, the basis coefficients $\{Z_1^1, \ldots, Z_{N_1}^1\}$ are random samples from a random process whose mean is $\bar{Z}^1$ and covariance Σ, and $\{Z_1^2, \ldots, Z_{N_2}^2\}$ are random samples from the same random process with mean $\bar{Z}^2$ and the same Σ. The sample means formed from each group will be

$$\hat{\bar{Z}}^1 = \frac{1}{N_1}\sum_{i=1}^{N_1} Z_i^1, \quad \hat{\bar{Z}}^2 = \frac{1}{N_2}\sum_{j=1}^{N_2} Z_j^2 \tag{23}$$

and the pooled (common) sample covariance

$$\hat{\Sigma} = \frac{1}{N_1 + N_2 - 2}\Big(\sum_{i=1}^{N_1}(Z_i^1 - \hat{\bar{Z}}^1)\,(Z_i^1 - \hat{\bar{Z}}^1)^T + \sum_{j=1}^{N_2}(Z_j^2 - \hat{\bar{Z}}^2)\,(\hat{Z}_j^2 - \hat{\bar{Z}}^2)^T\Big). \tag{24}$$

Then, to establish a hypothesis test of the two group means assuming an unknown but common covariance, the null hypothesis is

$$\mathcal{H}_0 : \bar{Z}^1 = \bar{Z}^2, \tag{25}$$

and the Hotelling's T^2 statistic (for two samples) is

$$T^2 \doteq \frac{N_1 N_2}{N_1 + N_2}(\hat{\bar{Z}}^1 - \hat{\bar{Z}}^2)^T\,\hat{\Sigma}^{-1}\,(\hat{\bar{Z}}^1 - \hat{\bar{Z}}^2). \tag{26}$$

The basis coefficients $\{Z_1^1, \ldots, Z_{N_1}^1\}$ are distributed according to $\mathcal{N}(\bar{Z}^1, \Sigma)$, and $\{Z_1^2, \ldots, Z_{N_2}^2\}$ according to $\mathcal{N}(\bar{Z}^2, \Sigma)$. The sample means $\hat{\bar{Z}}^1$ and $\hat{\bar{Z}}^2$ are distributed according to $\mathcal{N}(\bar{Z}^1, (1/N_1)\Sigma)$ and $\mathcal{N}(\bar{Z}^2, (1/N_2)\Sigma)$, respectively. Consequently, $\sqrt{N_1 N_2/(N_1+N_2)}\,(\hat{\bar{Z}}^1 - \hat{\bar{Z}}^2)$ is distributed according to $\mathcal{N}(0,\Sigma)$ under the null hypothesis. Following Anderson (1958), p. 109, $(N_1 + N_2 - 2)\hat{\Sigma}$ is distributed as $\sum_{i=1}^{N_1+N_2-2} X_i X_i^T$, where X_i is distributed according to $\mathcal{N}(0,\Sigma)$. Thus, T^2 has an F dis-

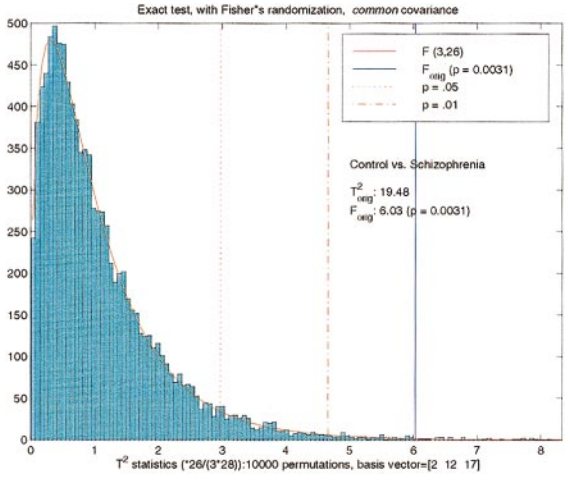

FIG. 7. Empirical distribution $\hat{F}$ from randomized Fisher's test with 10,000 group permutations, between the group of control and schizophrenia subjects. Basis vectors 2, 12, 17 are selected. The $P = 0.0031$ value shown is calculated from Eq. (33). Also shown are (i) $\hat{F}(T^2)$ value (solid blue line) of the control-versus-schizophrenia group comparison; (ii) theoretical F distribution (solid red curve) with (3,26) degrees of freedom superimposed on the empirical distribution; and (iii) $P = 0.05$ (red dotted line) and $P = 0.01$ (red dot-dash line) for reference.

tribution, and the null hypothesis $\mathcal{H}_0$ is rejected with a significance level α if

$$T^2 \geq \frac{(N_1 + N_2 - 2)K}{N_1 + N_2 - K - 1} F^*_{K,N_1+N_2-K-1}(\alpha), \quad (27)$$

where $F^*_{K,N_1+N_2-K-1}(\alpha)$ denotes the upper 100α% point of the $F_{K,N_1+N2-K-1}$ distribution, and K is the total number of basis functions used in calculating the T^2 statistics.

When the deformation vector fields are not assumed to be Gaussian, we have used Fisher's randomized permutation method to obtain the significance level of null hypothesis rejection. In Appendix C we give an example for such a treatment.

ASYMMETRY BETWEEN NORMALS AND SCHIZOPHRENIA

Logistic regressions based on χ^2 scores (SAS Institute Inc., 1989) performed on the two groups of coefficients (control and schizophrenia groups) indicate that linear combinations of a subset of the basis functions suffice to describe the difference between the two groups. Among those combinations, the set {2,12,17} is used to produce the results presented here. Other combinations result in similar outcomes.

For each subject, using the subset of basis functions, we calculate the log-likelihood ratio:

$$\Lambda = -\frac{1}{2}(Z_i - \hat{\bar{Z}}^{\text{schiz}})^T \hat{\Sigma}^{-1}(Z_i - \hat{\bar{Z}}^{\text{schiz}}) + \frac{1}{2}(Z_i - \hat{\bar{Z}}^{\text{ctrl}})^T \hat{\Sigma}^{-1}(Z_i - \hat{\bar{Z}}^{\text{ctrl}}), \quad (28)$$

depicted in Fig. 5a. Here, the symbols of vector coefficients represent the coefficient vectors with the selected components only (i.e., Z_i is the vector coefficient for subject i using only the 2nd, 12th, and 17th components, and similarly, $\hat{\bar{Z}}^{\text{ctrl}}$ and $\hat{\bar{Z}}^{\text{schiz}}$ are the sample means of the coefficient vectors using the above components for the control and schizophrenia groups, respectively). The log-likelihood ratios Λ give rise to a classification scheme under two hypotheses: Under H_0 (when $\Lambda < 0$) the sufficient statistics is Gaussian distributed with mean μ_0 and variance σ_0^2; Under H_1 (when $\Lambda > 0$), mean μ_1 and variance σ_1^2. Figure 5b shows the operating characteristics under these two hypotheses. The mean and standard deviation for each distribution are shown under the distribution curves.

In Table 5 we summarize the statistical test for the difference in asymmetry patterns between the control and schizophrenia groups. We conclude that this difference is statistically significant in distinguishing the two groups. The locations of this difference can be visualized in ways described in previous sections (see Figs. 1–3).

ASYMMETRY VECTOR FIELDS SYNTHESIS

In this section, we finally establish the correspondence between the subsets of basis functions and the asymmetry patterns they represent. If we express the asymmetry vector fields in the selected subset of basis functions, we can visualize the "action" of these basis functions. We note from Eqs. (15)–(17) that if K is the total number of basis functions used to express the asymmetry vector fields, the mean asymmetry vector field for any group g of N_g subjects can be calculated as

$$\hat{\bar{u}}^g = \frac{1}{N_g}\sum_{i=1}^{N_g} u_i^g = \frac{1}{N_g}\sum_{i=1}^{N_g}\sum_{k=1}^{K} < \mathrm{u}_\mathrm{i}^\mathrm{g}, \phi_\mathrm{k} > \phi_k = \sum_{k=1}^{K}\left(\frac{1}{N_g}\sum_{i=1}^{N_g} Z_i^{g,k}\right)\phi_k, = \sum_{k=1}^{K} \hat{\bar{Z}}^{g,k}\phi_k, \quad (29)$$

where $\hat{\bar{Z}}^{g,k}$ is the mean coefficient associated with the kth basis function for group g. Therefore, a subset of basis functions will produce (or reproduce) a mean asymmetry field using the selected subset of basis functions. Further, the difference of two mean asymmetry fields can be similarly reproduced by

$$\hat{\bar{u}}^1 - \hat{\bar{u}}^2 = \sum_{k=1}^{N} (\hat{\bar{Z}}^{l,k} - \hat{\bar{Z}}^{2,k})\phi_k. \quad (30)$$

In Fig. 6 we visualize the difference in the mean asymmetry fields expanded using the subset basis functions {2,12,17} for the control and schizophrenia groups. Note the similarity between Figs. 6a and 6b, which represents the normal component map, i.e., difference in the mean asymmetry fields expanded using the *entire* set of basis functions.

DISCUSSION

We have developed visualization and statistical characterization techniques for studying the asymmetry of brain structures such as the hippocampus. We have also developed a precise mathematical definition of asymmetry as a vector field. Obviously, zero asymmetry does not necessarily mean *normal* in a clinical sense. We therefore have proposed a statistical measure of asymmetry, which uses PCA to capture the "action" of asymmetry vector fields of normal and patient populations. The statistical analysis of the hippocampal vector fields then identifies the locations of normative right–left hippocampal asymmetry, as well

TABLE 5

Difference of Asymmetry Patterns: Control vs Schizophrenia

	Selected basis functions	Significance of difference
Control ($N = 15$) vs Schizophrenia ($N = 15$)	2,12,17	$P = 0.0029$ ($F = 6.03$, $df = 3,26$)

as in a group of schizophrenia subjects. Even though the asymmetry patterns between these two groups are highly similar, the statistical comparison of these patterns using PCA reveals a statistically significant group difference. The visualization techniques show that this difference occurs in the purple areas in Fig. 3b (top row) and in the red areas in the bottom row. In an atlas of the human hippocampus, Duvernoy showed the external surface of the hippocampus situated in a peel-away anatomy, viewed from above (Duvernoy, 1988) (Fig. 2, p. 15). The subiculum labeled there exactly corresponds to the subiculum delineated in our work (see Appendix A for a detailed anatomical delineation of the template hippocampus used here, which includes the subiculum). From Fig. 3 we can observe that the difference in the asymmetry patterns between the two groups is such that if the control subjects on the average have a thinner subiculum on the left side, then this "thinning" effect is more pronounced in the schizophrenia subjects on the average (i.e., schizophrenia subjects have an exaggerated asymmetries compared to the controls).

Neuronal connections from the hippocampal formations to the entorhinal cortex have been found to originate in CA1 and the subiculum (Witter *et al.*, 2000). Numerous texts have detailed explanations of afferent and efferent circuitry involving the hippocampus and the subiculum (Nieuwenhuys *et al.*, 1988; Suzuki and Eichenbaum, 2000; Burwell, 2000). Functionally, while most functional imaging studies in the medial temporal lobe have been able to activate hippocampus and parahippocampal gyrus (Schacter and Wagner, 1999), few researchers have been able to directly observe activation of the subiculum. In a study of six normal subjects, Gabrieli *et al.* (1997) were able to selectively activate the subiculum, during retrieval of previously shown drawings, therefore raising the possibility that the subiculum plays a role in memory. Our findings of asymmetry patterns in the subiculum suggest that the specific subregion of the hippocampus may be affected in schizophrenia.

In assessing hippocampal asymmetry, the mathematically defined reflection plane is defined with respect to the left and right hippocampi alone. Other definitions of the reflection plane may involve defining a mathematical midsagittal plane that considers all the brain structures on either side (see Ardekani *et al.*, 1997, for example). However, to use this plane to assess *hippocampal asymmetry* will most likely introduce an extra rotation and translation. In other words, while we have concentrated on the asymmetry of hippocampal shape, asymmetry between left and right brain hemispheres as a whole may be different. The hippocampus develops both as itself and as part of its surrounding brain environment. Therefore, assessing asymmetry in both ways may shed light on the development of diseases such as schizophrenia.

The method of studying asymmetry presented here is based on the assumption that we already have obtained the transformation vector fields from an anatomical atlas to the subjects. As a result, we have the surfaces of the brain structure-of-interest available in the population. These surfaces, which correspond to each other and to the template surface, could come from the HDBM algorithm used here or from other brain mapping methods (Thompson and Toga, 1996). Also, this method is not limited to the hippocampus, and it is readily applicable to other brain structures as long as we have a valid surface model for those structures. For example, this method can be applied to study the asymmetry of gyral surfaces mapped from a common anatomical atlas (Joshi *et al.*, 1999).

Furthermore, these methods should allow us to investigate the neurobiology of neuropsychiatric disorders other than schizophrenia. Normal brain development follows a "normal" asymmetric pattern, and therefore neurodevelopmental disorders such as autism and attention deficit hyperactivity disorder may also be associated with disturbances in the normal pattern of brain structure asymmetries. Also, normal patterns of brain structure asymmetry may render one hemisphere or the other more vulnerable to neurodegenerative processes, even if the processes are presumed to be ubiquitous. In our pilot work on AD (Csernansky *et al.*, 2000), we showed that early stage AD could be distinguished from healthy aging using similar methods of hippocampal shape analysis. Studies of the interaction between AD and normal patterns of brain asymmetry are under way.

APPENDIX A

Anatomical Delineations of the Template Hippocampus

In the template, the most posterior slice containing the hippocampus is defined when the hippocampus

first appears adjacent to the trigone of the lateral ventricle. A narrow band of gray matter along the medial aspect of the trigone opens to a thicker complex of gray matter and is separated from the trigone by a strip of white matter, i.e., the junction of the fimbria and fornix. The coronal slice shows an elongated shape to the gray matter complex, because of the transverse orientation of the hippocampal tail. This complex is the cornu ammonis (CA), dentate gyrus, and subiculum. The long stretch of cortex extending horizontally from the medial aspect of the CA is seen best in the coronal plane. However, it is difficult to select a point of separation because the superior component of the CA does not extend medially far enough to be the landmark of the medial border of the hippocampus, the inferior component of CA is continuous with the subiculum, and there is no gross anatomical separation of the subiculum, presubiculum, and parasubiculum, the latter-most being part of the parahippocampal gyrus. For these reasons, the subiculum and CA are included together in the measured volume called hippocampus, as has been done by others (Shenton *et al.*, 1992; Zipursky *et al.*, 1994), and the inferior border of the CA–subiculum is continued medially with a straight horizontal line across the cortex of the parahippocampal gyrus. The cortex below this line is thus considered the parahippocampal gyrus, and the cortex above this line included with the hippocampus.

Progressing anteriorly from the tail, the orientation of the hippocampus changes from the medial-to-lateral alignment of the tail to the posterior-to-anterior alignment of the body. Thus, the body is cross-sectioned in the coronal slices perpendicular to its long axis and appears to be divided by the white matter of the fimbria into a larger lower part, which is the CA–subiculum, and the smaller upper part formed by the tail of the caudate nucleus. The thalamus appears medial and superior to the subiculum–CA complex.

The thalamus and caudate nucleus form the superior borders of the hippocampus in its posterior aspect. The white matter boundary (alveus and fimbria) between the hippocampus and caudate nucleus as well as any CSF lateral to the hippocampus is not included. The superior and lateral borders of the hippocampal body and head are identified by the contrast against the white matter or CSF. The high signal of vessels at the medial aspect of the hippocampus is excluded from the hippocampus. Where the amygdala appears at the superior boundary of the hippocampal head, it as well as the white matter boundary are excluded. However, the vertical digitation of the hippocampal head which curves up and medial to the amygdala in coronal sections is included. The separation of the amygdala and hippocampus is best achieved by viewing sagittal and transverse sections.

APPENDIX B

High-Dimensional Brain Mapping

HDBM is a coarse-to-fine hierarchical procedure, which is defined by the biological problem itself, for generating the volume maps from the template to the targets. The first step is based on operator-identified anatomical landmarks (such as points and curves) in the template and target scans. These landmarks constraint the initial registration from the template to the target, adjusting for brain size, position, and orientation, as well as local regions surrounding the landmarks.

Having completed the "coarse," first step in the transformation, the scans are roughly aligned and attention is next turned to fine featured individual structures. The second step is to solve the nonlinear partial differential equations (PDE) that correspond to the Bayesian maximizer associated with the fluid dynamics formulation at each and every voxel of the image volume. Given a linear differential operator L (we have used the Navier equation $L = -a\nabla^2 - b\nabla\cdot\nabla + cI$, where a,b, and c are constants), the PDE $Lv(x, t) = b(x - u(x, t))$, $x \in \Omega$, $t \in [0, T]$, with boundary conditions $v(x, t) = 0$, $x \in \partial\Omega$, has a solution

$$v(x, t) = \frac{\partial u(x, t)}{\partial t} + \nabla^T u(x, t) v(x, t). \qquad (31)$$

This is the "velocity field," an auxiliary random field, whose time integral from 0 to T yields the 3D transformation field $u(x)$, $x \in \Omega$. Combining with the coarse map from step 1 and the identity map, we have the diffeomorphic transformations $h : \Omega \to \Omega$ (see Eq. (1)). For mathematical details as well as numerical solutions to PDE $Lv = b(x - u)$ see Christensen *et al.* (1996). Template anatomies (MR image volume, structure segmentation, or structure surface) are then mapped onto the targets through these transformation fields via trilinear interpolation.

There are limitations to any method, including HDBM. First, our methods depend heavily on the quality of the gray-scale image data. However, we are using the highest resolution MR images available that also contain data of uniform resolution for all the brain areas of interest. As better resolution scanning sequences become available, we will employ them and very likely increase the precision of our assessments. Also, nonuniformities in the MR image data due to poor calibration and field inhomogeneities may result in mismatches of gray and white matter, because our current tools are not driven solely by information about geometric structure. We have worked hard to control these sources of error using conventional strategies. In addition, we have recently begun to develop transfor-

mation tools that are driven solely by geometry and will therefore be invariant to nonuniformities in the MR images. Second, our methods are not entirely automatic, and the expertise of the expert neuroanatomist continues to play a key role. The expert creates the information in the template, and landmarks placed by experts may bias the initial manifold transformations. However, as regards the hippocampus, we have shown (Haller *et al.*, 1997) that the transformations are robust to this potential source of error (i.e., the automatic results were more repeatable than the results obtained from manual outlining).

APPENDIX C

Distribution-Free Statistical Test for Between-Group Comparisons

Recall from Section 5.3 that the basis coefficients $\{Z_1^1, \ldots, Z_{N_1}^1\}$ are random samples from a random process whose mean is $\bar{Z}^1$ and covariance is Σ, and $\{Z_1^2, \ldots, Z_{N_2}^2\}$ are random samples from the same random process with mean $\bar{Z}^2$ and the same Σ. The sample means formed from each group will be

$$\hat{\bar{Z}}^1 = \frac{1}{N_1}\sum_{i=1}^{N_1} Z_i^1, \quad \hat{\bar{Z}}^2 = \frac{1}{N_2}\sum_{j=1}^{N_2} Z_j^2$$

and the pooled (common) sample covariance

$$\hat{\Sigma} = \frac{1}{N_1 + N_2 - 2}\left(\sum_{i=1}^{N_1}(Z_i^1 - \hat{\bar{Z}}^1)(Z_i^1 - \hat{\bar{Z}}^1)^T + \sum_{j=1}^{N_2}(Z_j^2 - \hat{\bar{Z}}^2)(Z_j^2 - \hat{\bar{Z}}^2)^T\right).$$

To establish a hypothesis test of the two group means assuming an unknown but common covariance, the null hypothesis is

$$\mathcal{H}_0 : \bar{Z}^1 = \bar{Z}^2,$$

and the Hotelling's T^2 statistic (for two samples) as

$$T^2 \doteq \frac{N_1 N_2}{N_1 + N_2}(\hat{\bar{Z}}^1 - \hat{\bar{Z}}^2)^T \hat{\Sigma}^{-1}(\hat{\bar{Z}}^1 - \hat{\bar{Z}}^2). \quad (26)$$

In Fisher's method of randomization, for all permutations of the given two groups, new means and covariances are calculated. Monte Carlo simulations are used to generate a large number of uniformly distributed random permutations (a typical number is 10,000). The collection of T^2 statistics from each permutation gives rise to an empirical distribution $\hat{F}(52)$ according to (see Eq. (27))

$$F_{K, N_1+N_2-K-1} = \frac{N_1 + N_2 - K - 1}{(N_1 + N_2 - 2)K}\, T^2. \quad (32)$$

The null hypothesis that the two groups have equal means is rejected when

$$P = \int_{T^2}^{\infty} \hat{F}(f)\, df \quad (33)$$

falls below a predefined significance level (e.g., 0.05).

In Fig. 7 we plot the empirical distribution $\hat{F}$ from randomized Fisher's test with 10,000 group permutations, between the group of control and schizophrenia subjects. Basis vectors {2,12,17} are selected. The $P = 0.0031$ value shown is calculated from Eq. (33). Also shown are (i) $\hat{F}(T^2)$ value (solid blue line) of the control-versus-schizophrenia group comparison; (ii) theoretical F distribution (solid red curve) with (3,26) degrees of freedom superimposed on the empirical distribution; and (iii) $P = 0.05$ (red dotted line) and $P = 0.01$ (red dot-dash line) for reference.

We observe that the assumption of Gaussianity for the coefficient vectors are valid since the empirical distribution of the $\hat{F}$ statistics follows the F distribution curve.

ACKNOWLEDGMENTS

We thank Professor Ulf Grenander of Brown University for the contribution of asymmetry computation and Professor J. Philip Miller of Washington University School of Medicine for the contribution of statistical analysis. This work has been supported by NIH Grants MH56584 MH62130 and the George B. Couch Endowment at Washington University.

REFERENCES

Anderson, T. W. 1958. *An Introduction to Multivariate Statistical Analysis.* Wiley, New York.

Andreasen, N. C., Dennert, J. W., Olsen, S. A., and Damasio, A. R. 1982. Hemisphereic asymmetries and schizophrenia. *Am. J. Psychiatry* **139:** 427–430.

Ardekani, B. A., Kershaw, J., Braun, M., and Kanno, I. 1997. Automatic detection of the mid-sagittal plane in 3-d brain images [letter]. *IEEE Trans. Med. Imag.* **16:** 947–952.

Bullmore, E., Brammer, M., Harvey, I., Murray, R., and Ron, M. 1995. Cerebral hemispheric asymmetry revisited: Effects of handedness, gender and schizophrenia measured by radius of gyration in magnetic resonance images. *Psychol. Med.* **25:** 349–363.

Burwell, R. D. 2000. The parahippocampal region: Corticocortical connectivity. *Ann. N.Y. Acad. Sci.* **911:** 25–42.

Christensen, G. E., Joshi, S. C., and Miller, M. I. 1997. Volumetric transformation of brain anatomy. *IEEE Trans. Med. Imag.* **16**.

Christensen, G. E., Rabbitt, R. D., and Miller, M. I. 1994. 3D brain mapping using a deformable neuroanatomy. *Phys. Med. Biol.* **39:** 609–618.

Christensen, G. E., Rabbitt, R. D., and Miller, M. I. 1996. Deformable templates using large deformation kinematics. *IEEE Trans. Image Process.* **5:** 1435–1447.

Claudio, M., and Roberto, S. 1994. Using marching cubes on small machines. *Graphical Models Image Process.* **56:** 182–183.

Collins, D. L., Neelin, P., Peters, T. M., and Evans, A. C. 1994. Automatic 3d intersubject registration of MR volumetric data in standardized Talairach space. *J. Comput. Assist. Tomogr.* **18:** 192–205.

Cook, M. J., Fish, D. R., Shorvon, S. D., Straughan, K., and Stevens, J. M. 1992. Hippocampal volumetric and morphometric studies in frontal and temporal lobe epilepsy. *Brain* **115:** 1001–1015.

Csernansky, J. G., Joshi, S. C., Wang, L., Miller, J. P., and Miller, M. I. 1998. Hippocampal morphometry in schizophrenia by high dimensional brain mapping. *Proc. Natl. Acad. Sci.* **95:** 11406–11411.

Csernansky, J. G., Wang, L., Joshi, S. C., Miller, J. P., Gado, M., Kido, D., McKeel, D., Morris, J. C., and Miller, M. I. 2000. Early dat is distinguished from aging by high dimensional mapping of the hippocampus. *Neurology* **55:** 1636–1643.

Dickey, C. C., McCarley, R. W., Voglmaier, M. M., Niznikiewicz, M. A., Seidman, L. J., Hirayasu, Y., Fischer, I., Teh, E. K., Van Rhoads, R., Jakab, M., Kikinis, R., Jolesz, F. A., and Shenton, M. E. 1999. Schizotypal personality disorder and MRI abnormalities of temporal lobe gray matter. *Biol. Psychiatry* **45:** 1393–1402.

Duvernoy, H. M. 1988. *The Human Hippocampus: An Atlas of Applied Anatomy*, p. 15. Bergmann Verlag, Munich, Germany.

Eidelberg, D., and Galaburda, A. M. 1982. Symmetry and asymmetry in the human posterior thalamus. i. Cytoarchitectonic analysis in normal persons. *Arch. Neurol.* **39:** 325–332.

Gabrieli, J. D. E., Brewer, J. B., Desmond, J. E., and Glover, G. H. 1997. Separate neural bases of two fundamental memory processes in the human medial temporal lobe. *Science* **276:** 264–266.

Galaburda, A. M., LeMay, M., Kemper, T. L., and Geschwind, N. 1978. Right–left asymmetries in the brain. *Science* **199:** 852–856.

Galderisi, S., Mucci, A., Mignone, M. L., Bucci, P., and Maj, M. 1999. Hemispheric asymmetry and psychopathological dimensions in drug-free patients with schizophrenia. *Int. J. Psychophysiol.* **34:** 293–301.

Geschwind, N., and Levitsky, W. 1968. Human brain: Left–right asymmetries in the temporal speech region. *Science* **161:** 186–187.

Glicksohn, J., and Myslobodsky, M. S. 1993. The representation of patterns of structural brain asymmetry in normal individuals. *Neuropsychologia* **31:** 145–159.

Grenander, U. 1970. A unified approach to pattern analysis. *Adv. Comput.* **10:** 175–216.

Grenander, U. 1994. *General Pattern Theory*. Oxford Univ. Press, Oxford, England.

Grenander, U., and Miller, M. I. 1994. Representations of knowledge in complex systems. *J. R. Stat. Soc. B* **56:** 549–603.

Grenander, U., and Miller, M. I. 1998. Computational anatomy: An emerging discipline. *Q. Appl. Math.* **LVI:** 617–694.

Haller, J. W., Banerjee, A., Christensen, G. E., Gado, M., Joshi, S. C., Miller, M. I., Sheline, Y., Vannier, M. W., and Csernansky, J. G. 1997. 3d hippocampal morphometry by high dimensional transformation of a neuroanatomical atlas. *Radiology* **202:** 504–510.

Hirayasu, Y., Shenton, M. E., Salisbury, D. F., Dickey, C. C., Fischer, I. A., Mazzoni, P., Kisler, T., Arakaki, H., Kwon, J. S., Anderson, J. E., Yurgelun-Todd, D., Tohen, M., and McCarley, R. W. 1998. Lower left temporal lobe MRI volumes in patients with first-episode schizophrenia compared with psychotic patients with first-episode affective disorder and normal subjects. *Am. J. Psychiatry* **155:** 1384–1391.

Hogan, R. E., Mark, K. E., Wang, L., Joshi, S. C., Miller, M. I., and Bucholz, R. D. 1999. MR imaging deformation-based segmentation of the hippocampus in patients with mesial temporal sclerosis and temporal lobe epilepsy. *Epilepsia* **40(Suppl. 7):** 192.

Jack, C. R., Jr., Gehring, D. G., Sharbrough, F. W., Felmlee, J. P., Forbes, G., Hench, V. S., and Zinsmeister, A. R. 1988. Temporal lobe volume measurement from MR images: Accuracy and left–right asymmetry in normal persons. *J. Comput. Assist. Tomogr.* **12:** 21–29.

James, A. C., Crow, T. J., Renowden, S., Wardell, A. M., Smith, D. M., and Anslow, P. 1999. Is the course of brain development in schizophrenia delayed? Evidence from onsets in adolescence. *Schizophrenia Res.* **40:** 1–10.

Joshi, M., Cui, J., Doolittle, K., Joshi, S. C., Van Essen, D., Wang, L., and Miller, M. I. 1999. Brain segmentation and the generation of cortical surfaces. *NeuroImage* **9:** 461–476.

Joshi, S. C. 1997. *Large Deformation Diffeomorphisms and Gaussian Random Fields for Statistical Characterization of Brain Submanifolds*, Ph.D. thesis. Department of Electrical Engineering, Sever Institute of Technology, Washington University, St. Louis, MO.

Joshi, S. C., Miller, M. I., Christensen, G. E., Banerjee, A., Coogan, T. A., and Grenander, U. 1995. Hierarchical brain mapping via a generalized Dirichlet solution for mapping brain manifolds. In *Proceedings of the SPIE's 1995 International Symposium on Optical Science, Engineering, and Instrumentation, San Diego, CA*, Vol. 2573 of *Vision Geometry IV*, pp. 278–289.

Joshi, S. C., Miller, M. I., and Grenander, U. 1997. On the geometry and shape of brain sub-manifolds. *Int. J. Patt. Recog. Artificial Intelligence, special issue on Magnetic Resonance Imaging* **11:** 1317–1343.

Kopp, N., Michel, F., Carrier, H., Biron, A., and Duvillard, P. 1977. Hemispheric asymmetries of the human brain. *J. Neurol. Sci.* **34:** 349–363.

Kulynych, J. J., Vladar, K., Fantie, B. D., Jones, D. W., and Weinberger, D. R. 1995. Normal asymmetry of the planum temporale in patients with schizophrenia. Three-dimensional cortical morphometry with MRI. *Br. J. Psychiatry* **166:** 742–749.

Kulynych, J. J., Vladar, K., Jones, D. W., and Weinberger, D. R. 1993. Three-dimensional surface rendering in MRI morphometry: A study of the planum temporale. *J. Comput. Assist. Tomogr.* **17:** 529–535.

Lawson, J. A., Nguyen, W., Bleasel, A. F., and Pereira, J. K. 1998. Ilae-defined epilepsy syndromes in children: Correlation with quantitative MRI. *Epilepsia* **39:** 1345–1349.

Lee, J. W., Reutens, D. C., Dubeau, F., Evans, A., and Andermann, F. 1995. Morphometry in temporal lobe epilepsy. *Magn. Reson. Imag.* **13:** 1073–1080.

LeMay, M. 1976. Morphological cerebral asymmetries of modern man, fossil man, and nonhuman primate. *Ann. N. Y. Acad. Sci.* **280:** 349–266.

LeMay, M. 1977. Asymmetries of the skull and handedness: Phrenology revisited. *J. Neurol. Sci.* **32:** 243–253.

LeMay, M., and Kido, D. 1978. Asymmetries of the cerebral hemispheres on computed tomograms. *J. Comput. Assist. Tomogr.* **2:** 471–476.

Loftus, W. C., Tramo, M. J., Thomas, C. E., Green, R. L., Nordgren, R. A., and Gazzaniga, M. S. 1993. Three-dimensional quantitative analysis of hemispheric asymmetry in the human superior temporal region. *Cereb. Cortex* **3:** 348–355.

Lotspeich, L. J., and Ciaranello, R. D. 1993. The neurobiology and genetics of infantile autism. *Int. Rev. Neurobiol.* **35:** 87–129.

Luchins, D. J., Weinberger, D. R., and Wyatt, R. J. 1979. Schizophrenia: Evidence of a subgroup with reversed cerebral asymmetry. *Arch. Gen. Psychiatry* **36:** 1309–1311.

Luxenberg, J. S., May, C., Haxby, J. V., Grady, C., Moore, A., Berg, G., White, B. J., Robinette, D., and Rapoport, S. I. 1987. Cerebral metabolism, anatomy, and cognition in monozygotic twins discordant for dementia of the Alzheimer type. *J. Neurol. Neurosurg. Psychiatry* **50:** 333–340.

Miller, M., Banerjee, A., Christensen, G., Joshi, S., Khaneja, N., Grenander, U., and Matejic, L. 1997. Statistical methods in computational anatomy. *Stat. Methods Med. Res.* **6:** 267–299.

Miller, M., Christensen, G., Amit, Y., and Grenander, U. 1993. Mathematical textbook of deformable neuroanatomies. *Proc. Natl. Acad. Sci.* **90**.

Moossy, J., Zubenko, G. S., Martinez, A. J., and Rao, G. R. 1988. Bilateral symmetry of morphologic lesions in Alzheimer's disease [see comments]. *Arch. Neurol.* **45:** 251–254.

Mottaghy, F. M., Shah, N. J., Krause, B. J., Schmidt, D., Halsband, U., Jancke, L., and Muller-Gartner, H. W. 1999. Neuronal correlates of encoding and retrieval in episodic memory during a paired-word association learning task: A functional magnetic resonance imaging study. *Exp. Brain Res.* **128:** 332–342.

Nieuwenhuys, R., Voogd, J., and van Huijzen, C. 1988. *The Human Central Nervous System: A Synopsis and Atlas*, third ed. Springer Verlag, Berlin.

Peled, S., Gudbjartsson, H., Westin, C. F., Kikinis, R., and Jolesz, F. A. 1998. Magnetic resonance imaging shows orientation and asymmetry of white matter fiber tracts. *Brain Res.* **780:** 27–33.

Pieniadz, J. M., and Naeser, M. A. 1984. Computed tomographic scan cerebral asymmetries and morphologic brain asymmetries: Correlation in the same cases post mortem. *Arch. Neurol.* **41:** 403–409.

Pruessner, J. C., Li, L. M., Serles, W., Pruessner, M., Collins, D. L., Kabani, N., Lupien, S., and Evans, A. C. 2000. Volumetry of hippocampus and amygdala with high-resolution MRI and three-dimensional analysis software: Minimizing the discrepancies between laboratories. *Cereb. Cortex* **10:** 433–442.

SAS Institute Inc. 1989. *SAS/STAT User's Guide*, Version 6, fourth ed., Vol. 2. SAS Institute Inc., Cary, NC.

Schacter, D. L., and Wagner, A. D. 1999. Medial temporal lobe activations in fMRI and PET studies of episodic encoding and retrieval. *Hippocampus* **9:** 7–24. [Review]

Shenton, M. E., Kikanis, R., Jolesz, F. A., Pollak, S. D., LeMay, M., Wible, C. G., Hokama, H., Martin, J., Metcalf, D., Coleman, M., and McCarley, R. W. 1992. Abnormalities of the left temporal lobe and thought disorder in schizophrenia: A qualitative magnetic resonance imaging study. *N. Engl. J. Med.* **327:** 604–612.

Suzuki, W. A., and Eichenbaum, H. 2000. The neurophysiology of memory. *Ann. N. Y. Acad. Sci.* **911:** 175–191.

Szeszko, P. R., Robinson, D., Alvir, J. M., Bilder, R. M., Lencz, T., Ashtari, M., Wu, H., and Bogerts, B. 1999. Orbital frontal and amygdala volume reductions in obsessive–compulsive disorder. *Arch. Gen. Psychiatry* **56:** 913–919.

Thompson, P. M., Moussai, J., Zohoori, S., Goldkorn, A., Khan, A. A., Mega, M. S., Small, G. W., Cummings, J. L., and Toga, A. W. 1998. Cortical variability and asymmetry in normal aging and Alzheimer's disease. *Cereb. Cortex* **8:** 492–509.

Thompson, P. M., Schwartz, C., and Toga, A. W. 1996. High-resolution random mesh algorithms for creating a probabilistic 3d surface atlas of the human brain. *NeuroImage* **3:** 19–34.

Thompson, P. M., and Toga, A. W. 1996. A surface-based technique for warping three-dimensional images of the brain. *IEEE Trans. Med. Imag.* **15:** 402–417.

Tien, A. Y., Eaton, W. W., Schlaepfer, T. E., McGilehrist, I. K., Menon, R., Powers, R., Aylward, E., Barta, P., Strauss, M. E., and Pearlson, G. D. 1996. Exploratory factor analysis of MRI brain structure measures in schizophrenia. *Schizophrenia Res.* **19:** 93–101.

Weinberger, D. R., Luchins, D. J., Morihisa, J., and Wyatt, R. J. 1982. Asymmetrical volumes of the right and left frontal and occipital regions of the human brain. *Ann. Neurol.* **11:** 97–100.

Wible, C. G., Shenton, M. E., Hokama, H., Kikinis, R., Jolesz, F. A., Metcalf, D., and McCarley, R. W. 1995. Prefrontal cortex and schizophrenia: A quantitative magnetic resonance imaging study. *Arch. Gen. Psychiatry* **52:** 279–288.

Wilcoxon, F. 1945. Individual comparisons by ranking methods. *Biomet. Bull.* **1:** 80–83.

Witter, M. P., Wouterlood, F. G., Naber, P. A., and Van Haeften, T. 2000. Anatomical organization of the parahippocampal–hippocampal network. *Ann. N. Y. Acad. Sci.* **911:** 1–24.

Wu, J. C., Buchsbaum, M. S., Hershey, T. G., Hazlett, E., Sicotte, N., and Johnson, J. C. 1991. PET in generalized anxiety disorder. *Biol. Psychiatry* **29:** 1181–1199.

Zipursky, R. B., Marsh, L., Lim, K. O., DeMent, S., Shear, P. K., Sullivan, E. V., Murphy, G. M., Csernansky, J. G., and Pfefferbaum, A. 1994. Volumetric MRI assessment of temporal lobe structures in schizophrenia. *Biol. Psychiatry* **35:** 501–516.